

# A Numerical Solution for the Time Variant Maxwell Equations using a Discontinuous Galerkin Method

Juan G. Fuentes, Sergio I. Valdez, Salvador Botello

*Research Center of Mathematics (CIMAT A.C.), Computational Sciences Department  
Jalisco S/N, Col. Valenciana CP:36240 Guanajuato Gto., Mexico  
{juan.fuentes,ivvan,botello}@cimat.mx*

**Abstract.** In this work a parallel scheme to solve the dynamic Maxwell's equations is presented, in order to simulate an electromagnetic wave in a two-dimensional domain composed of distinct dielectric materials and subject to boundary conditions. In this approach a Discontinuous Galerkin Finite Element Method (DG-FEM) is used to compute the solution over a discretized domain of non-overlapping straight-sided elements. In contrast to continuous Galerkin methods, the core of the simulation relies on a set of elementwise calculations instead of a global processing. These local calculations are computed simultaneously in a shared memory environment with the parallel framework proposed, taking advantage of the discontinuous nature of the solver implemented.

**Keywords:** Discontinuous Galerkin, Maxwell's equations, Finite Element Method, Parallel Computing.

## 1 Introduction

### 2

In the area of Computational Electromagnetics (CEM), Discontinuous Galerkin Methods (DGM) has become an efficient alternative for simulation of high frequency electromagnetic (EM) waves on geometrically complex domains, at an affordable computational cost. The main advantages of DGM over continuous schemes and conventional Finite Differences in Time Domain (FDTD) methods consist in an effective handling of unstructured grids and a high accuracy approximation. In essence, DGM combine the best features of Finite Element methods (FEM) and Finite Volume (FV) methods, providing a high capability of delivering high-order accuracy solutions in conjunction with local conservation.

In conventional continuous FEM, globally defined mass and stiffness matrices need to be computed, thus computationally expensive sparse linear systems are solved. For time-dependent problems, such schemes present a clear disadvantage in comparison with Finite Differences (FDTD) and Finite Volume (FV) methods. In DGM, the information used to calculate the solution over each element involves solely communication with directly neighbouring elements, via numerical fluxes. As a result, mass matrices and gradient operators are only locally defined, offering an efficient and natural parallelization scheme, especially for solving problems on unstructured triangular grids, even with high order triangulations and complex geometries, such as curved face elements.

Two remarkable methods regarding electromagnetic simulation using DGM found in literature are the nodal triangle-based Spectral Element method (SE), proposed by Giraldo and Warburton [5], in which the Lagrange polynomials are constructed from nodal sets based on an electrostatics principle formulated by Hesthaven [6], and the unstructured polymorphic hp-finite elements approach of Hesthaven and Warburton [7], where the feasibility of simulating EM scattering problems using mixed-element grids is demonstrated. In this work an application of a Discontinuous Galerkin formulation in a grid composed of non-overlapping straight-sided elements is presented. Likewise, a parallel scheme using a shared memory environment is implemented and evaluated in terms of time consumption and efficiency.

In the next section, the differential form of Maxwell's equations, including a non-dimensional form and boundary conditions is introduced. In the third section, a strong and weak forms of DGM, as well as its application to Maxwell's equations are formulated. In section 4, the explicit expressions for calculating the electric and magnetic fields are derived. In section 5, a two-dimensional test case is presented and evaluated in order to validate the performance of the solver implemented. In section 6, the parallel scheme is presented, along with a performance evaluation over a two-dimensional test case. Finally, concluding remarks are given in section 7.

### 3 Maxwell's Equations

#### a. Formulation

Maxwell's equations are formulated from experimental results with the purpose of describing the interactions between time-variant electric and magnetic fields of an *electromagnetic phenomena*. The differential forms of Maxwell's equations are given as follows:

$$\nabla \times \mathbf{E} = -\frac{\partial \mathbf{B}}{\partial t}, \quad (1)$$

$$\nabla \times \mathbf{H} = \mathbf{J} - \frac{\partial \mathbf{D}}{\partial t}, \quad (2)$$

where  $\mathbf{E}$ ,  $\mathbf{H}$  are the electric and magnetic field intensities respectively, and  $\mathbf{B}$ ,  $\mathbf{D}$  correspond to the electric and magnetic flux densities.  $\mathbf{J}$  is an electric current density source term. All these variables are time-dependent vector fields in  $\mathfrak{R}^n$ . Intensities and flux terms relate each other by the following constitutive relations:

$$\mathbf{D} = \epsilon \mathbf{E}, \mathbf{B} = \mu \mathbf{H}, \mathbf{J} = \sigma \mathbf{E}, \quad (3)$$

where  $\epsilon$  is called *permittivity* constant, it measures how certain material resists an electric field. The *permeability* constant  $\mu$  measures the resistance to a magnetic field. The intrinsic *conductivity*  $\sigma$  measures the resistance to an electric current intensity. For simplicity, this work is focused on isotropic, linear, time-invariant materials. However, in practice, anisotropic or lossy media present complex permittivity and permeability parameters, which are dependent on the position, temperature, or the wave frequency.

By substituting the constitutive relations of (3) in equations (1) and (2), we obtain two expressions that uniquely relate  $\mathbf{E}$  and  $\mathbf{H}$ :

$$\mu \frac{\partial \mathbf{H}}{\partial t} = -\nabla \times \mathbf{E}, \quad (4)$$

$$\epsilon \frac{\partial \mathbf{E}}{\partial t} = \nabla \times \mathbf{H} - \sigma \mathbf{E}. \quad (5)$$

In this work a numerical method for obtaining a time domain solution of (4) and (5) is given, i.e. a method for calculating the vector quantities  $\mathbf{E}$  and  $\mathbf{H}$  such that equations (4) and (5) are satisfied in a certain time interval within a domain  $\Omega$ .

#### b. Normalization

Since all variables in (4) and (5) are physical dimensional quantities, a normalization operation needs to be applied in order to handle similar dimensionalities. Here, we introduce the vacuum speed of light as normalization factor, defined as  $c_0 = \frac{1}{\sqrt{\epsilon_0 \mu_0}} \simeq 3 \times 10^8$ , and a normalized expression for Maxwell's equations is considered instead of the dimensional form:

$$\mu_r \frac{\partial \tilde{\mathbf{H}}}{\partial \tilde{t}} = -\nabla \times \tilde{\mathbf{E}}, \quad (6)$$

$$\epsilon_r \frac{\partial \tilde{\mathbf{E}}}{\partial \tilde{t}} = \nabla \times \tilde{\mathbf{H}} - \sigma \tilde{\mathbf{E}}. \quad (7)$$

where the non-dimensional quantities are defined as

$$\tilde{\mathbf{H}}(\tilde{\mathbf{x}}, \tilde{t}) = \frac{\mathbf{H}(\mathbf{x}, t)}{H_0}, \quad \tilde{\mathbf{E}}(\tilde{\mathbf{x}}, \tilde{t}) = Z_0^{-1} \frac{\mathbf{E}(\mathbf{x}, t)}{H_0}, \quad x = \frac{x}{\lambda}, \quad \tilde{t} = \frac{c_0 t}{\lambda}$$

Here,  $H_0$  is a reference magnetic field strength,  $Z_0 = \sqrt{\mu_0/\epsilon_0} \simeq 120\pi$  ohms is the vacuum impedance, and  $\lambda$  could be the wavelength of the phenomenon of interest. The relative permittivity and permeability constants  $\epsilon_r, \mu_r$  are given by  $\mu = \mu_0\mu_r$  and  $\epsilon = \epsilon_0\epsilon_r$ , where  $\epsilon_0, \mu_0$  are the vacuum permittivity and permeability, respectively.

### c. Boundary Conditions

An electromagnetic wave can exist in a region composed by two distinct materials, in such cases, the interface separating those regions must satisfy the so called boundary conditions. In electromagnetics, boundary conditions can be classified in *dielectric-dielectric* or *dielectric-conductor*, depending on the dielectric constants of the materials that form the interface. For *dielectric-dielectric* conditions, it is established that the tangential components of the electric field  $\mathbf{E}$  in both sides of the interface must be equal:

$$\hat{\mathbf{n}} \times \mathbf{E}^- = \hat{\mathbf{n}} \times \mathbf{E}^+, \quad (8)$$

and in the case of dielectric-conductor boundaries, the tangential component of the electric field in the dielectric side vanishes at the interface of the conductor:

$$\hat{\mathbf{n}} \times (\mathbf{E}^-) = 0 \Rightarrow \mathbf{E}^- = 0, \quad (9)$$

## 4 Discontinuous Galerkin Method

### a. General Formulation

The Discontinuous Galerkin approach is derived from the general form of the conservation law, also known as continuity equation, which describes the transport of a conservative quantity  $\mathbf{q}$ :

$$\frac{\partial \mathbf{q}}{\partial t} + \nabla \cdot \mathbf{F}(\mathbf{q}) = \mathbf{S}. \quad (10)$$

Here,  $\mathbf{F}(\mathbf{q})$  is a flux vector which describes the local transport of  $\mathbf{q}$ , and  $\mathbf{S}$  is a source term which represents an increase/decrease in the conservative quantity. The residual of (10) is multiplied by a test function  $\psi$  and integrated over a domain  $\Omega$ :

$$\int_{\Omega} \psi \left[ \frac{\partial \mathbf{q}}{\partial t} + \nabla \cdot \mathbf{F}(\mathbf{q}) - \mathbf{S}(\mathbf{q}) \right] d\Omega = 0 \quad (11)$$

As in many finite element techniques, it is assumed that the domain of interest  $\Omega$  can be discretized into a set of straight-faced, non-overlapping elements  $\Omega_e$ , such that  $\bigcup \Omega_e \approx \Omega$ . the set of edges located in the boundary of  $\Omega$  is defined as  $\Gamma$ , and  $\Sigma$  is defined as the set of inner edges. Referring to Fig. 1, the following elementwise relations are implied:

$$\Gamma_e = \Omega_e \cap \Gamma, \quad \Sigma_e = \Omega_e \cap \Sigma, \quad \partial\Omega_e = \Gamma_e \cup \Sigma_e.$$

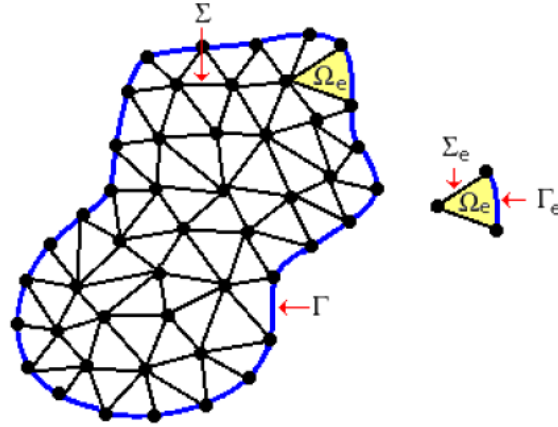


**Fig. 1.** Domain discretization in straight-faced, non-overlapping finite elements.

Then, (11) can be approximated by elementwise integrals:

$$\sum_e \left[ \int_{\Omega_e} \psi \frac{\partial q}{\partial t} d\Omega_e + \int_{\Omega_e} \psi (\nabla \cdot \mathbf{F}(\mathbf{q})) d\Omega_e - \int_{\Omega_e} \psi \mathbf{S}(\mathbf{q}) d\Omega_e \right] = 0. \quad (12)$$

Applying the divergence theorem gives:

$$\int_{\Omega_e} \psi \frac{\partial q}{\partial t} d\Omega_e + \int_{\partial\Omega_e} \psi (\mathbf{F}(\mathbf{q}) \cdot \hat{\mathbf{n}}) ds - \int_{\Omega_e} \nabla \psi \cdot \mathbf{F}(\mathbf{q}) d\Omega_e - \int_{\Omega_e} \psi \mathbf{S}(\mathbf{q}) d\Omega_e = 0, \quad (13)$$

where  $\hat{\mathbf{n}}$  is an outward pointing unit vector normal to the element surface.

The DGM does not impose continuity conditions on the solution. As can be observed in (13), since the surface integrals are defined over each element interface, the flux of  $\mathbf{q}$  through such boundaries is discontinuous. Then, the above scheme needs to be modified to enforce a coupling between neighbouring elements.

The state variable  $\mathbf{q}$  can be represented as a linear combination of piecewise polynomial functions or shape functions  $N$  and nodal coefficients  $q_j$  defined over each element:

$$q_N = \sum_{j=1}^n q_j N_j$$

In Galerkin methods, the test functions  $\psi$  are equal to the shape functions:

$$\int_{\Omega_e} N_i \frac{\partial q_N}{\partial t} d\Omega_e + \int_{\partial\Omega_e} N_i (\mathbf{F}(\mathbf{q}_N) \cdot \hat{\mathbf{n}}) ds - \int_{\Omega_e} \nabla N_i \cdot \mathbf{F}(\mathbf{q}_N) d\Omega_e - \int_{\Omega_e} N_i \mathbf{S}(\mathbf{q}_N) d\Omega_e = 0. \quad (14)$$

In order to enforce the coupling between neighbouring elements, the surface integral in (14) is replaced by a numerical flux  $F^*(q_N^-, q_N^+)$  to correct the flux discontinuity (*weak form*):

$$\int_{\Omega_e} \left[ N_i \frac{\partial q_N}{\partial t} - \nabla N_i \cdot \mathbf{F}(\mathbf{q}_N) - N_i \mathbf{S}(\mathbf{q}_N) \right] d\Omega_e = - \int_{\partial\Omega_e} N_i F^*(q_N^-, q_N^+) \cdot \hat{\mathbf{n}} ds. \quad (15)$$

Finally, the strong form of (15) is obtained by applying the divergence theorem again on the second term of the left side:

$$\int_{\Omega_e} N_i \left[ \frac{\partial q_N}{\partial t} - \nabla \cdot \mathbf{F}(q_N) - \mathbf{S}(q_N) \right] d\Omega_e = \int_{\partial\Omega_e} N_i [F(q_N) - F^*(q_N^-, q_N^+)] \cdot \hat{n} ds. \quad (16)$$

## b. Formulation for Maxwell's Equations

From the above formulation, Maxwell's equations can be expressed in conservation form, considering the electric and magnetic field terms as the state variables:

$$\epsilon_r \frac{\partial E_N}{\partial t} - \nabla \times H_N - S(E_N) = 0. \quad (17)$$

$$\mu_r \frac{\partial H_N}{\partial t} + \nabla \times E_N - S(H_N) = 0. \quad (18)$$

Then, applying the strong DGM formulation to (17) and (18) gives:

$$\int_{\Omega_e} N_i \left[ \epsilon_r \frac{\partial E_N}{\partial t} - \nabla \times H_N - S(E_N) \right] d\Omega_e = \int_{\partial\Omega_e} N_i [F(H_N) - F^*(H_N^-, H_N^+)] \cdot \hat{n} ds. \quad (19)$$

$$\int_{\Omega_e} N_i \left[ \mu_r \frac{\partial H_N}{\partial t} - \nabla \times E_N - S(H_N) \right] d\Omega_e = \int_{\partial\Omega_e} N_i [F(E_N) - F^*(E_N^-, E_N^+)] \cdot \hat{n} ds. \quad (20)$$

For simplification, a single penalization term is introduced:

$$P(q_N^-, q_N^+) = \hat{n} \cdot [F(q_N) - F^*(q_N^-, q_N^+)],$$

then:

$$\int_{\Omega_e} N_i \left[ \epsilon_r \frac{\partial E_N}{\partial t} - \nabla \times H_N - S(E_N) \right] d\Omega_e = \int_{\partial\Omega_e} N_i P(H_N^-, H_N^+) ds, \quad (21)$$

$$\int_{\Omega_e} N_i \left[ \mu_r \frac{\partial H_N}{\partial t} - \nabla \times E_N - S(H_N) \right] d\Omega_e = \int_{\partial\Omega_e} N_i P(E_N^-, E_N^+) ds. \quad (22)$$

In Discontinuous Galerkin Methods, the choice of the numerical flux is a central element of the scheme and it is also where knowledge of the dynamics of the problem can be introduced. A number of DGM variants can be obtained by selecting different types of numerical fluxes. Although there are several schemes that could work in most cases, the upwind flux approach is one of the most used techniques for wave-type equations:

$$P(H_N^-, H_N^+) = \bar{Z}^{-1} \mathbf{n} \times (Z^+ [H_N] - \mathbf{n} \times [E_N]) \quad (23)$$

$$P(E_N^-, E_N^+) = \bar{Y}^{-1} \mathbf{n} \times (\mathbf{n} \times [H_N] - Y^+ [E_N]) \quad (24)$$

where:

$$\begin{aligned} [E_N] &= E_N^+ - E_N^- & [HN] &= H_N^+ - H_N^- \\ \bar{Z} &= Z^+ + Z^- & \bar{Y} &= Y^+ + Y^- \end{aligned}$$

Here, the superindex (-) refers to the local element, and (+) refers to a neighbour element. Z and Y are the impedance and the admittance of the material respectively, defined as

$$Z^\pm = \frac{1}{Y^\pm} = \sqrt{\frac{\mu_r^\pm}{\epsilon_r^\pm}}$$

## 5 Explicit form and Timestepping

### a. Time Discretization

For temporal discretization, it is known that classical fourth order Runge-Kutta approach (RK4) requires four extra storage arrays for every iteration. A more efficient alternative is using a low-storage version of the fourth order explicit Runge-Kutta scheme (LSERK) [8] to deal with time integration. Let be the time derivative at certain moment defined as follows:

$$\frac{\partial q^n}{\partial t^n} = F(q^n, t^n)$$

where  $q$  is the state variable and  $n$  is the current time step. Then, the time stepping process to obtain the value of the state variable at the next timestep is given by the next five-stage update algorithm:

$$\begin{aligned} p^0 &= q^n, \\ i \in [1, \dots, 5]: &\begin{cases} k^i = a^i k^{i-1} + \Delta t F(p^{i-1}, t^n + ci \Delta t), \\ p^i = p^{i-1} + b_i k^i, \end{cases} \\ q^{n+1} &= p^5. \end{aligned} \quad (25)$$

The coefficients needed in the LSERK method are given in Table 1. Although this approach implies additional function evaluations and an extra storage array  $k$ , such drawbacks are overcome by allowing a larger stable timestep  $\Delta t$ .

**Table 1.** Coefficients for the low-storage five-stage fourth-order ERK method (LSERK).

$i$	$a_i$	$b_i$	$c_i$
1	0	0.149659021999229	0
2	-0.417890474499852	0.379210312999627	0.149659021999229
3	-1.192151694642677	0.822955029386982	0.370400957364205
4	-1.697784692471528	0.699450455949122	0.622255763134443
5	-1.514183444257156	0.153057247968152	0.958282130674690

### b. Semidiscrete Form and Elementwise Operations

Now, in order to define an elementwise explicit semidiscrete expression for the electric and magnetic components, equations (21) and (22) are rewritten in matricial form:

$$\epsilon_r M \left( \frac{\partial E^n}{\partial t^n} \right) - K \times H^{n-1} - M[S^{n-1}(E)] = F[P^{n-1}(H^-, H^+)], \quad (26)$$

$$\mu_r M \left( \frac{\partial H^n}{\partial t^n} \right) + K \times E^{n-1} - M[S^{n-1}(H)] = F[P^{n-1}(E^-, E^+)]. \quad (27)$$

where the various elementwise operators are defined as follows:

$$\begin{aligned}
 M_{ij} &= \int_{\Omega^e} N_i(x)N_j(x) \, d\Omega^e \\
 K_{ij} &= \int_{\Omega^e} N_i(x)\nabla N_j(x) \, d\Omega^e \\
 F_{iL} &= \oint_{\partial\Omega^e} N_i(x)N_L(x) \, ds.
 \end{aligned} \tag{28}$$

Here,  $M$ ,  $K = (K_x, K_y, K_z)$ , and  $F$  are the mass matrix, stiffness matrices and surface matrix respectively. Finally, rewriting (26) and (27) in fully explicit form yields:

$$\frac{\partial E^n}{\partial t^n} = \frac{1}{\epsilon_r} M^{-1} [K \times H^{n-1} + M [S^{n-1}(E)] + F [P^{n-1}(H^-, H^+)]] \quad , \tag{29}$$

$$\frac{\partial H^n}{\partial t^n} = \frac{1}{\mu_r} M^{-1} [-K \times E^{n-1} + M [S^{n-1}(H)] + F [P^{n-1}(E^-, E^+)]] \quad , \tag{30}$$

and then combining (29) and (30) with the LSERK scheme given in (25) the explicit update for the electric and magnetic components is complete.

## 6 Two-dimensional Test Case

### a. Polarization Modes

Since  $E$  and  $H$  are vector quantities, they represent three direction components each. Then, solving Maxwell's equations in three dimensions implies finding six unknowns in total at every time step  $\Delta t$ . A simpler case involves solving the Maxwell's equations in their two dimensional form. In Electromagnetics, two polarization modes are distinguished for problems involving waveguides, in which the field components are orthogonal to the direction of the scattering wave.

In the Transverse Magnetic Mode (TM), the fields are restricted to the components  $E_z$ ,  $H_x$  and  $H_y$ :

Maxwell's equations:

$$\begin{aligned}
 \mu \frac{\partial H_x}{\partial t} &= -\frac{\partial E_z}{\partial y} \\
 \mu \frac{\partial H_y}{\partial t} &= \frac{\partial E_z}{\partial x} \\
 \epsilon \frac{\partial E_z}{\partial t} &= \left( \frac{\partial H_y}{\partial x} - \frac{\partial H_x}{\partial y} \right) - \sigma E_z
 \end{aligned}$$

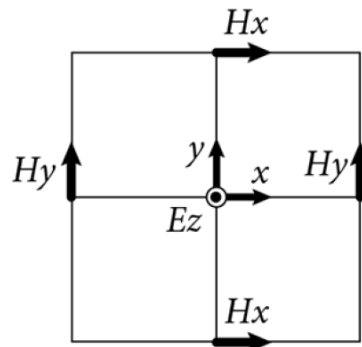
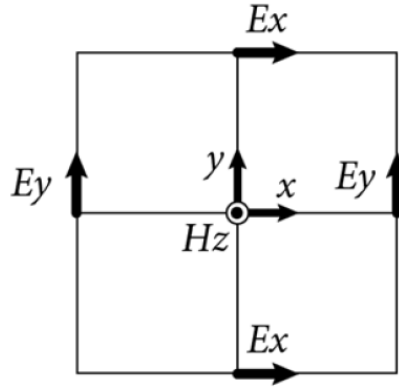


Fig. 2. Transverse Magnetic Mode

In the Transverse Electric Mode (TE), the fields are restricted to the components  $H_z$ ,  $E_x$  and  $E_y$ :

Maxwell's equations:

$$\begin{aligned} \epsilon \frac{\partial E_x}{\partial t} &= \frac{\partial H_z}{\partial y} - \sigma E_x \\ \epsilon \frac{\partial E_y}{\partial t} &= -\frac{\partial H_z}{\partial x} - \sigma E_y \\ \mu \frac{\partial H_z}{\partial t} &= -\left(\frac{\partial E_y}{\partial x} - \frac{\partial E_x}{\partial y}\right) \end{aligned}$$



**Fig. 3.** Transverse Electric Mode.

## b. Test Case

**c.** As a first example, let us consider the solution of Maxwell's equations in TM mode within a two-dimensional vacuum cavity. In TM mode formulation, the explicit equations for calculating the update terms are simplified as follows:

$$\begin{aligned} \frac{\partial E_z^n}{\partial t^n} &= \frac{1}{\epsilon_r} M^{-1} [K_x H_y^{n-1} - K_y H_x^{n-1} + P^{n-1} (E_z^-, E_z^+)] \\ \frac{\partial H_x^n}{\partial t^n} &= \frac{1}{\mu_r} M^{-1} [K_y E_z^{n-1} + P^{n-1} (H_x^-, H_x^+)] \\ \frac{\partial H_y^n}{\partial t^n} &= \frac{1}{\mu_r} M^{-1} [K_x E_z^{n-1} + P^{n-1} (H_y^-, H_y^+)] \end{aligned} \quad (31)$$

In order to validate the performance of the implementation proposed, the following test problem is solved inside a metallic air-filled cavity, with  $\Omega = [1, 1]^2$ , and the approximate solution obtained is compared with the exact solution:

$$\begin{aligned} H^x(x, y, t) &= -\frac{\pi n}{\omega} \sin(m\pi x) \cos(n\pi y) \sin(\omega t), \\ H^y(x, y, t) &= \frac{\pi m}{\omega} \cos(m\pi x) \sin(n\pi y) \sin(\omega t), \\ E^z(x, y, t) &= \sin(m\pi x) \cos(n\pi y) \sin(\omega t), \end{aligned}$$

where the resonance frequencies  $\omega$ , are given as

$$\omega = \pi \sqrt{m^2 + n^2}, \quad (m, n) > 0.$$

For simplicity, we take  $m = n = 1$ .

For the boundary conditions, a mirror principle are used to simulate reflective boundary conditions, based on assigning  $E_z^+ = -E_z^-$  such that  $E_z^+ + E_z^- = 0$ , this is enforced by assigning  $[E_z] = 2E_z^-$  at all boundary points.

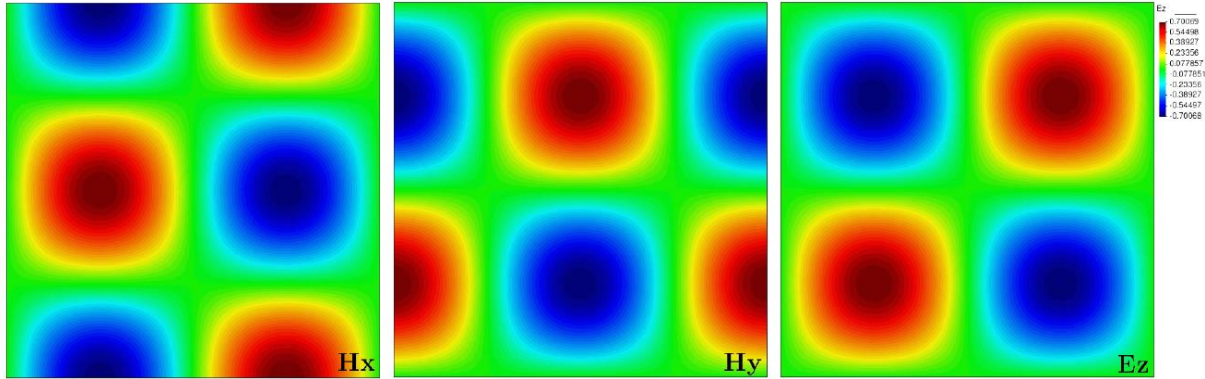


**Fig. 4.** Image capture of the result obtained in the test problem. From left to right:  $H_x$ ,  $H_y$ ,  $E_z$ .

#### d. Performance Evaluation

In order to evaluate the stability of the solver implemented, two performance tests are conducted. The first test consisted in discretizing the domain  $\Omega$  using different quantities of elements and comparing the approximate and exact solution per node, using a mean square error (MSE) as comparative measurement. In Fig. 5, MSE error is shown for two different space discretizations, the left plot are generated from a discretization of 200 straight-sided triangular elements, while the right plot refers to a discretization of 3200 elements.

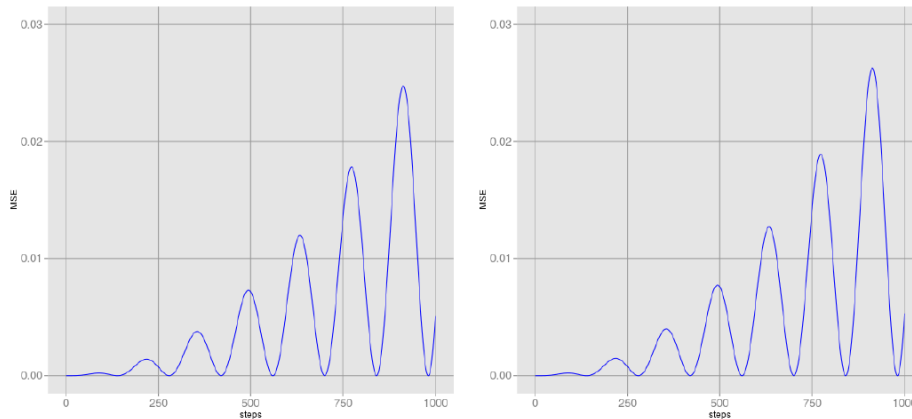


**Fig. 5:** MSE for two different domain discretizations during 1000 time steps of 0.005 sec. Left: 200 triangular elements. Right: 3200 triangular elements.

As can be observed in Fig. 5, a good approximation of exact solution is obtained in both cases. It is however interesting to point out how the error accumulates as the steps increase and the phase of the exact solution changes over time. The second test consisted is using different timestepping  $\Delta t$  for a constant domain discretization. In Fig. 6 the MSE error is shown for two different time discretizations, the left plot refers to a time step of 0.025 sec., while the right plot represents a time step of 0.0025 sec.

It can be concluded from the results obtained by distinct time and spatial discretizations, that as long as an appropriate time step  $\Delta t$  is chosen (i.e.  $\Delta t$  satisfies the Courant criterion for the specified scattering problem), the stability and accuracy of the solver is ensured. Thus, it is evident the solver's ability to obtain a high-order approximation, due to the FEM-based method implemented, as well as a high stability to a wide range of time steps due to the Runge-Kutta scheme used.

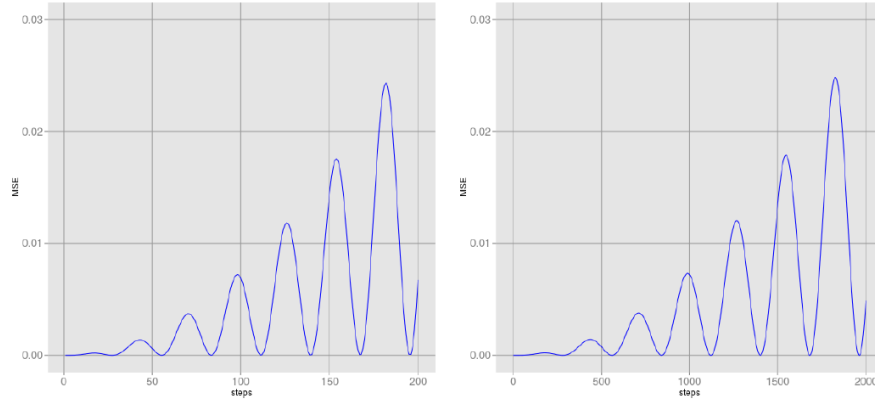


**Fig. 6:** MSE for two different time discretizations. Left:  $\Delta t = 0.025$ . Right:  $\Delta t = 0.0025$ .

## 7 Parallel Scheme

As mentioned at the beginning, the discontinuous nature of the method allows only local access to memory, which has a significant advantage over conventional continuous methods, since at each iteration each section of memory is accessed only by one processor, so that no collisions occur. In addition, the synchronization points are significantly reduced, since the final update of the state variables is done only at the end of each iteration. This makes the DGM ad-hoc for a parallel scheme, either for shared or distributed memory environments.

Once the DGM formulation and its application to the Maxwell’s Equations is described, the main steps of the DGM solver are depicted in Fig. 7. As we are dealing with straight faced elements over isotropic media, the element matrices are constant and they only have to be computed once and stored during the iterative process. At the right side of every computation block, the approximate percent of time execution is indicated, and as we can see, most of the time are consumed by the field derivatives calculation.

Since all of the blocks inside the time step iterative process are computed elementwise, we propose a parallel scheme in which all elementwise calculations are performed in parallel for each block, such as depicted in Fig. 8. The only moment when information is shared among element neighborhoods is when the numerical fluxes are being calculated. Then, before that computation block is initiated, the state variables need to be fully updated from last iteration.

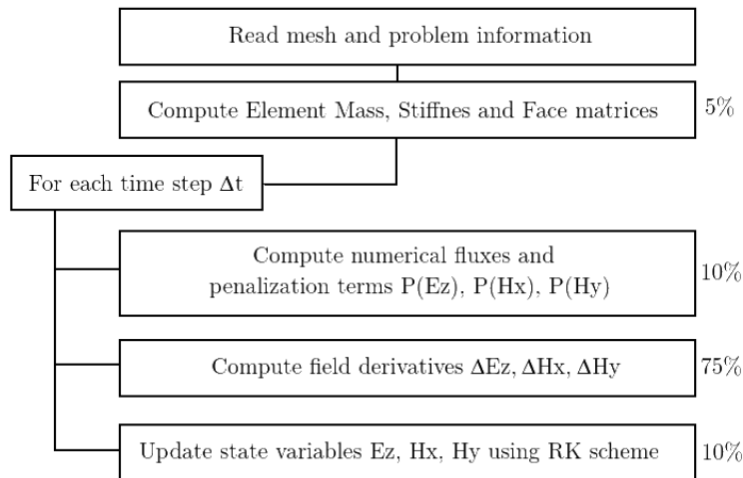


**Fig.7:** Main steps of the DGM iterative algorithm.

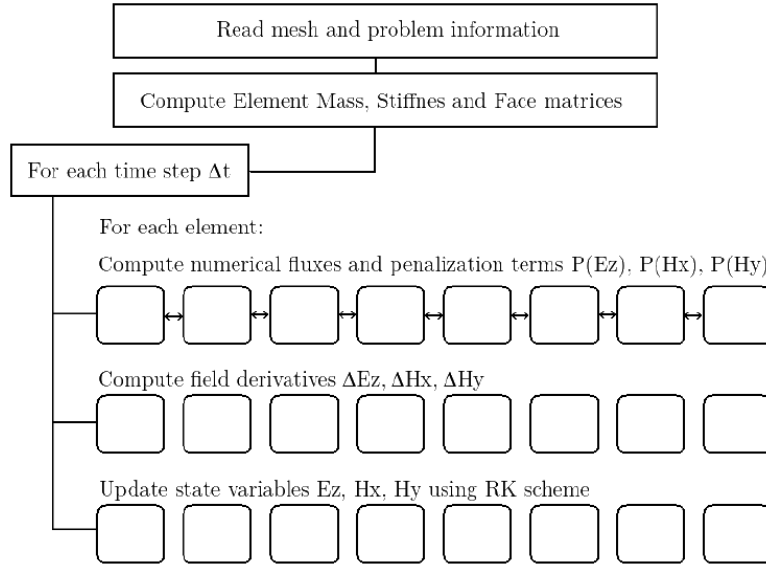


**Fig.8:** Parallel scheme of the main steps inside the time stepping process.

In order to evaluate the efficiency of the parallel scheme proposed, the electric field component of a TM mode electromagnetic wave is simulated within a two-dimensional domain  $\Omega \in [-1, 1]$  which includes some dielectric materials so the reflection effect can be observed, as shown in left side of Fig. 9. A sinusoidal wave with origin at  $(0, 0)$  is introduced as source term in the scattering analysis. In this test case, a 3200 six-node triangular mesh is generated and the simulation is run over 50 sec. in 10000 steps. In Fig. 10 execution time and speed-up plots are shown from one to 24 cores:

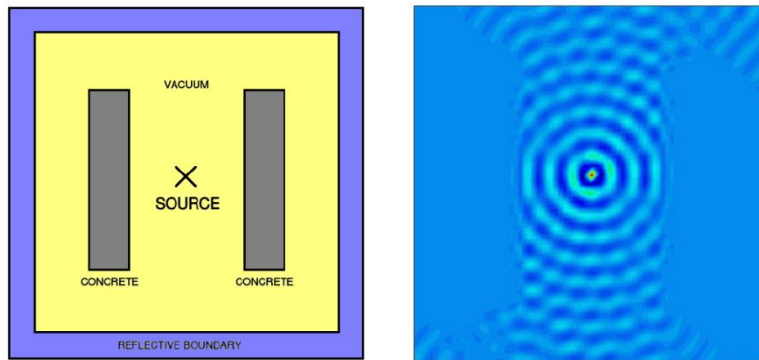


**Fig.9:** Material disposition and simulation screenshot.

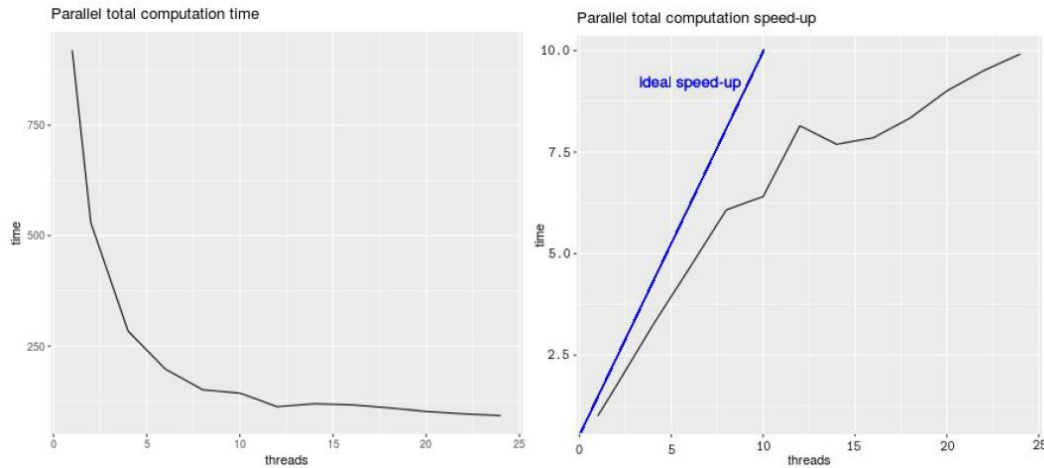


Fig.10: Efficiency assessment of the parallel scheme.

## 8 Conclusions

A convergent, accurate, highly parallelizable method for electromagnetic wave simulation in two-dimensional domains has been presented in this work, as well as an effective approach for representation of dielectric materials in space. From the formulation presented, the method is readily scalable to three-dimensional domains.

Summarizing the results presented in this work, it is concluded that DG-FEM methods can effectively solve EM scattering problems, and provide a good approximation of a solution for the Maxwell's Equations over a discretized domain. Also it is showed good performance in scattering analysis with dielectric boundaries, in which an analytic solution could not easily be found. It is also concluded that high efficiency is achieved when this scheme is implemented in a shared memory environment, due to the local processing and coupling via numerical fluxes.

As future work, several engineering applications will be approached, such as topological design of dielectric materials and high frequency transmitters, in which several optimization methods will be applied with this electromagnetic solver as a cost evaluator.

## References

1. A. Klöckner, T. Warburton, J. Bridge, J.S. Hesthaven: Nodal discontinuous Galerkin methods on graphics processors. *Journal of Computational Physics* 228 (2009) 7863-7882
2. J. S. Hesthaven, T. Warburton: Nodal HighOrder Methods on Unstructured Grids: TimeDomain Solution of Maxwells Equations, *Journal of Computational Physics* 181: 186-221 (2002).
3. J.S. Hesthaven, T. Warburton: *Nodal Discontinuous Galerkin Methods: Algorithms, Analysis, and Applications*. Springer Texts in Applied Mathematics 54. Springer Verlag, New York, 2008.
4. F.X. Giraldo, J.B. Perot, P.F. Fischer: A spectral element semi-Lagrangian (SESL) method for the spherical shallow water equations, *Journal of Computational Physics* 190 (2003) 623-650.
5. F.X. Giraldo, T. Warburton: A nodal triangle-based spectral element method for the shallow water equations on the sphere, *Journal of Computational Physics* 207 (2005) 129-150.
6. J.S. Hesthaven: From electrostatics to almost optimal nodal sets for polynomial interpolation in a simplex, *SIAM Journal on Numerical Analysis* 35 (1998) 655-676.
7. T. Warburton: *Application of the discontinuous galerkin method to Maxwells equations using unstructured polymorphic hp-finite elements*. Lecture Notes in Computational Science and Engineering, Springer-Verlag, New York, 2000.
8. M.H. Carpenter, C. Kennedy: Fourth-order 2N-storage Runge-Kutta schemes, NASA Report TM 109112, NASA Langley Research Center, 1994.
9. David I. Ketcheson: *Runge-Kutta Methods with Minimum-Storage Implementations*. Department of Applied Mathematics, University of Washington, Seattle.